AirCargoChallenge 2022

Technical Report

Team #18

Chicken Wings CTU

Content

1. Introduction

1.1 Main objective

The ACC 2022 flight mission demands us to design and build UAV that is capable of short take off, maximum payload transportation, high rate of climb and high cruise speed. This report describes our vision of UAV that will meet the required criteria.

1.2 Design Approach

The design approach of aircraft is based on experience gained in previous projects and competitions that we attended. Our UAV has been fully designed within student's semester projects and bachelor's theses in close cooperation with faculty of Mechanical Engineering at CTU (Czech Technical University in Prague).

Our approach includes:

- Minimizing aerodynamic resistance by reducing drag of landing gear
- Minimizing construction weight by utilizing 3d print and CFRP
- Making compact cargo bay by placing part of the payload in the wing
- Using high-lift devices

1.3 The setback of our plans

On April 23 there was a fire in our workshop that destroyed everything that we had. We will try to produce the same airplane as we designed but due to many factors that include shipping time of material and equipment we might be forced to slightly alter our design.

Figure 1: Fire of our workshop

2. Project management

2.1 Time management

We created the time schedule of the design process to complete the project successfully. The schedule in form of Gantt chart includes most of the important activities. Support and non-technical activities (e. g. negotiations with sponsors, workspace arranging, marketing activities) are not included and took place simultaneously to the design process. Compared to previous seasons, the designing process was one year longer due to the postponed competition.

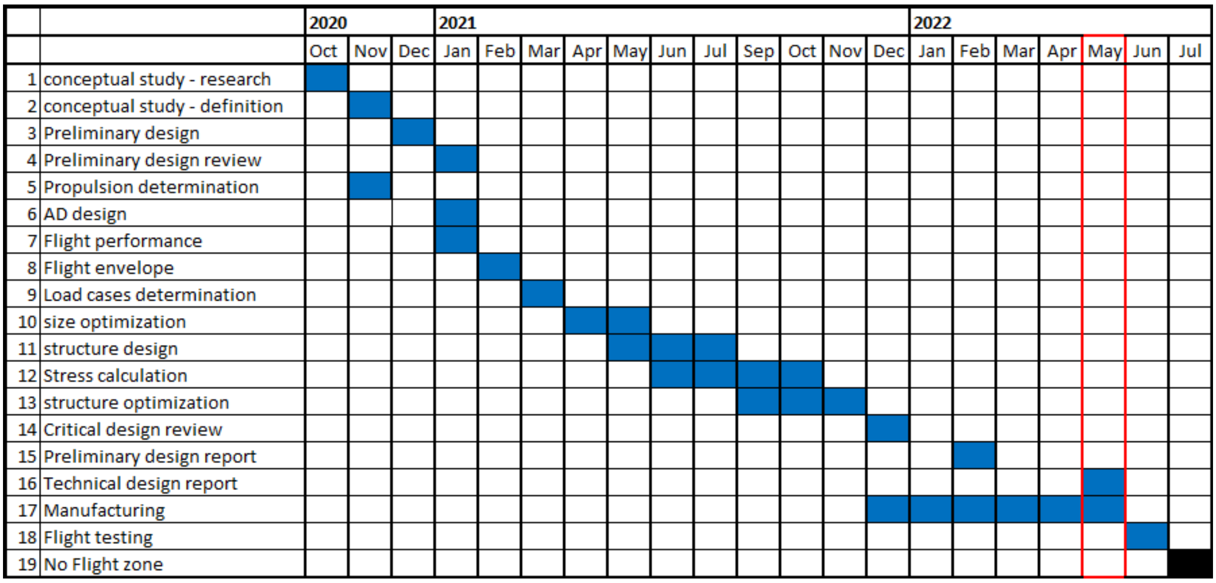

Figure 2: Gantt diagram

2.2 Cost report

The costs of our project are depicted in Table 1 and Figure 2. Since the beginning of the academic year, we have kept an estimate of the overall costs to guarantee enough resources throughout the season. Our estimates of production costs would be slightly over-estimated. Compared to the estimate, the real production costs were lower by 7,5 %.

However, our workshop caught fire and all our equipment and semi-finished prototypes got damaged. This event has caused some additional expenses which need to be included in our cost report. These cover the material and electronics which got damaged and needed to be bought again.

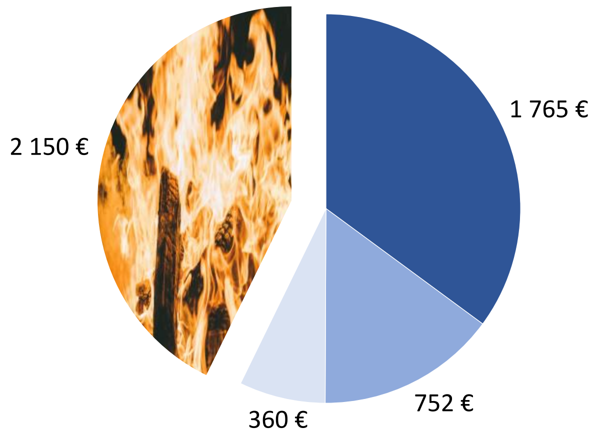

Figure 3: Ratio of expenses

Expenses	Est. Costs (10/2021) [€]	Real Cost [€]	Sponsoring [€]	
Production costs	2000	1765	40,2%	709
Competition costs	752	752	-	-
Travel costs	360	360*	-	-
Subtotal:	**3112**	**2877 (2168**)**	**24,6%**	**709**
Extra costs due to fire	-	2150	9,6%	207
Total:	**3112**	**5027 (4111**)**	**18,2%**	**916**

**only estimation available ** including sponsorship*

Table 1: Cost report

3. Overall aircraft design

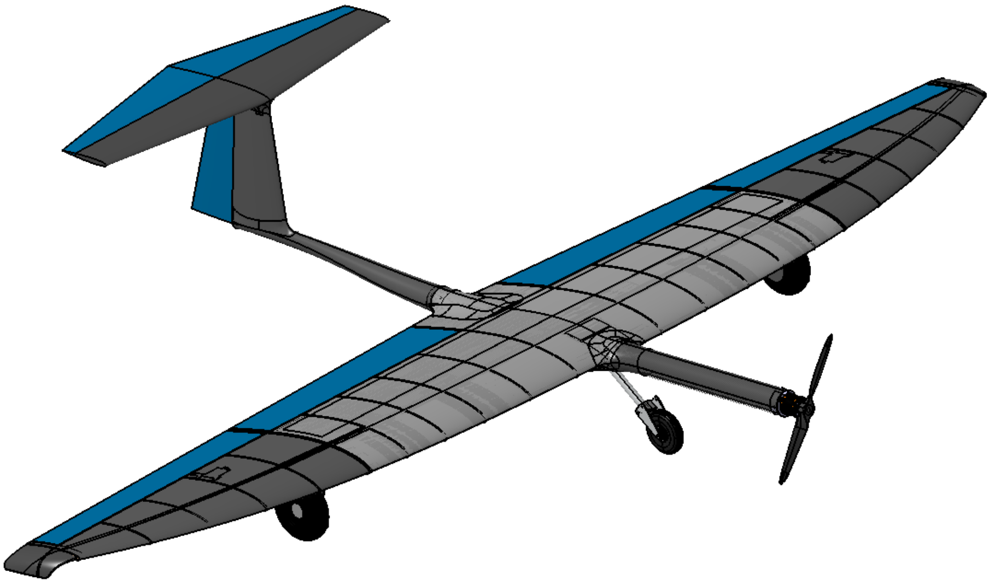

Figure 4: Aircraft model

Wing area	0,64	[m^2]
Wingspan	2,17	[m]
Length	1,40	[m]
Empty weight	3,0	[kg]
Horizontal tail volume	0,37	[-]
Vertical tail volume	0,024	[-]
Elevator lever arm	0,7	[m]
Wing airfoil	K3311, S8000	
Empennage airfoil	NACA 0009	

Table 2: Main aircraft dimensions

3.1 Aircraft configuration

3.1.1 Overall airplane configuration

The most conservative and verified configuration is the monoplane. The necessity of higher lift can be solved by high-lift devices and stability is ensured by the tail. This concept is also generally easier to design and manufacture. (ANDERSON, 1999). The simplest solution is a flying-wing configuration. It provides large cargo space while keeping low drag and good performance. However, it tends to be unstable due to its sensitivity to the location of centre of gravity. The most experimental considered configuration is the canard. The major advantage is that the aerodynamic force from the horizontal stabilizer is generated in the same direction as the lift on the main wing. On the other hand, it leads to unstable flight characteristics. The canard sizing is much more critical than aft tail sizing.

	Weight	**Stability**	**Maximum lift**	**Minimum drag**	**Σ**
Weight	0,3	0,2	0,4	0,1	1
Monoplane	3	5	5	3	4,2
Canard	3	3	3	3	3
Flying Wing	5	1	2	5	3

Table 3: Aircraft configuration trade study

3.1.2 Wing configuration

Due the very slim shape of the fuselage in the midwing section the aircraft is identified as high wing monoplane. Upper side of the wing is unobstructed by the fuselage. For the wing shape ellipse and trapezoid was considered. Lift distribution aspect and shape aspect for fitting the assembled aircraft into the rhombus shape box was better for the ellipse shape. On the other hand, trapezoid shape is easier to produce. However, ellipse has been chosen because thanks to our technology of production the more complex elliptic shape is equally difficult to produce.

Several types of flaps have been evaluated, like Fowler's flap or Junker's flap, but because of the previous experience and ease of production simple plain flap has been selected.

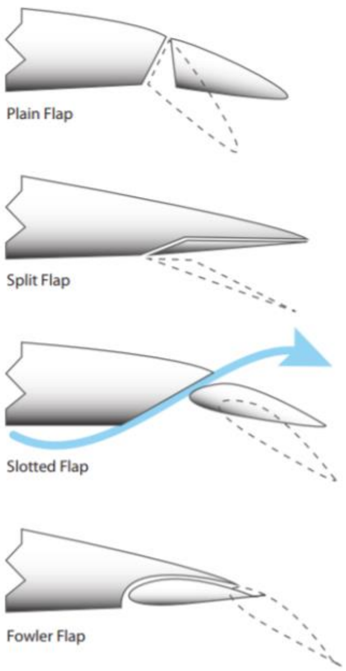

Figure 5: Different types of flaps

For the inner support structure of the wing simple 2 spars configuration has been selected, front spar to close torsion D-box over leading edge cover and to take majority of the bending loads. Secondary spar to help with bending loads and to support wing mechanisation like flaps and ailerons. In between both spars have been spread several ribs to reinforce the cover to prevent buckling or loss of stability from torsion loads. In place of wing split there are 3D printed inserts in the webbing of main spar to reinforce the spar and to accept connecting tube from aluminium alloy that connects wing and wingtips together and transfers the bending loads. On both sides if the wing splits are reinforced ribs and pin in between them to transfer the torsion loads.

3.1.3 Empennage configuration

We have considered 3 types of empennages: Conventional tail, T tail and V tail.

T – tail: The main advantage of T-tail is high control effectiveness caused by the placement of vertical stabilizer outside of effects of the disturbed airflow from the propeller. The main disadvantage of T-tail is the possibility of entering a deep stall while flying at high angle of attack.

V – tail: Instead of rudder and elevator v-tail uses ruddervators that function similarly but through a more complex control system. The main advantages are lower weight and less aerodynamic drag. The main disadvantage is the secondary tilt moment, which must be eliminated and overall complicated construction.

Conventional tail: provides appropriate stability and control. In most cases it leads to lightweight construction. The main disadvantage in this case is risk of damage when landing on the grass. (SLAVÍK, 1997)

	Control Effectiveness	Weight	Manufactu-rability	Drag	Stall behavior	Σ
Weight	0,3	0,2	0,2	0,1	0,2	1
Conven-tional	4	2	5	3	5	3,9
V-tail	3	5	3	5	4	3,8
T-tail	5	3	5	4	3	4,1

Table 4: Comparison of tail types

3.1.4 Cargospace design

We had considered two possibilities for cargo storage. Either we could put cargo in external cargo pod, or we could integrate it inside the wing.

Placing the cargo in external cargo pod would provide a suitable place for mounting a landing gear. Also it may be advantegeous to completely separate a cargo-space from wing. Its main disadvantage is its volume that would cause a increase of drag and also another support structure increase a empty weight.

Cargo inside the wing structure is the best according to aerodynamics because it does not interfere with it much. Due to lowering the perpendicular stability of airplane it is possible to reduce the wing area and therefore achieve another improvement of aerodynamical properties of the wing. Although it is not suited for all types of cargo because of the wing support structure.

After we took into consideration type of cargo and competition objective, we decided for cargo stored inside the wing. The rib's pitch was adapted in a way that the blood bags- fit between them and fix them in place so they cannot move during flight.

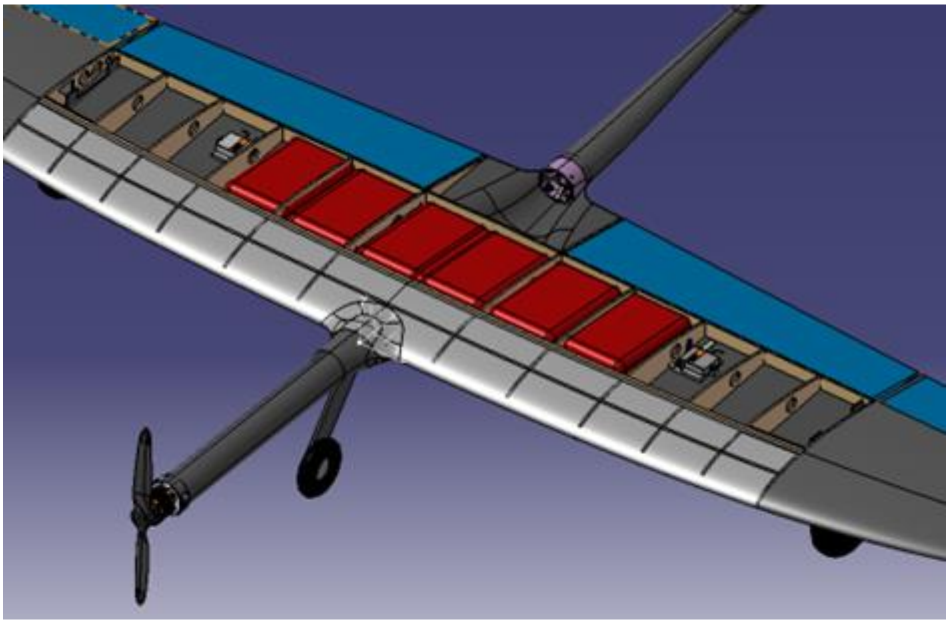

Figure 6: Storage of cargo in wing

3.1.5 Landing gear configuration

The most common landing gear configurations are the tricycle and the inverted tricycle. Deciding between the two, we took into account mainly stabilty on the ground. The classic tricycle was a simplier solution, but becouse of stability, we chose the inverted tricycle.

We calculated, that if we keep the weight of the landing gear below 400 grams, the reduced air resistance would compensate for the weight of the retraction mechanism. However, after the previously mentioned fire, we abandoned this concept due to time and budget constraints. Thus, we designed a simple fixed landing gear, equipped with suspension.

Based on the chosen reversed tricycle configuration we positioned the main landing gear on the underside of the wing, behind the center of gravity. We designed the legs and suspension with regard to manufacturability and simplicity. The wide gauge, although less suitable due to the stress it puts on the wing, was used becouse of the fixed shape of the cargo space.

The first iteration of the nose gear protruded vertically from the fuselage, with suspension mounted on a lever connected to the wheel. Suspension in the second concept was provided by a tube with a spring housed in a tube of larger diameter. The third version was mounted at an angle in the centerplane. Suspension was provided by a lever mechanism. We chose the third version using multi-criteria evaluation, mainly due to low stress on the connection between the centerplane and the fuselage during take off and landing.

	Load on fuselage	Landing leg strength	Weight	Design complexity	Σ
weight	0,5	0,2	0,2	0,1	1
vertical (shock absorber inside pipe)	2	5	5 (122 g)	2	3,2
vertical (shock absorber on lever)	1	4	5 (104 g)	4	2,7
sloped centerplane mounted	5	3	1 (252 g)	2	3,5

Table 5: Comparison of nose gear types

3.2 Structural design

konstrukční řešení důležitých uzlů, materiály,

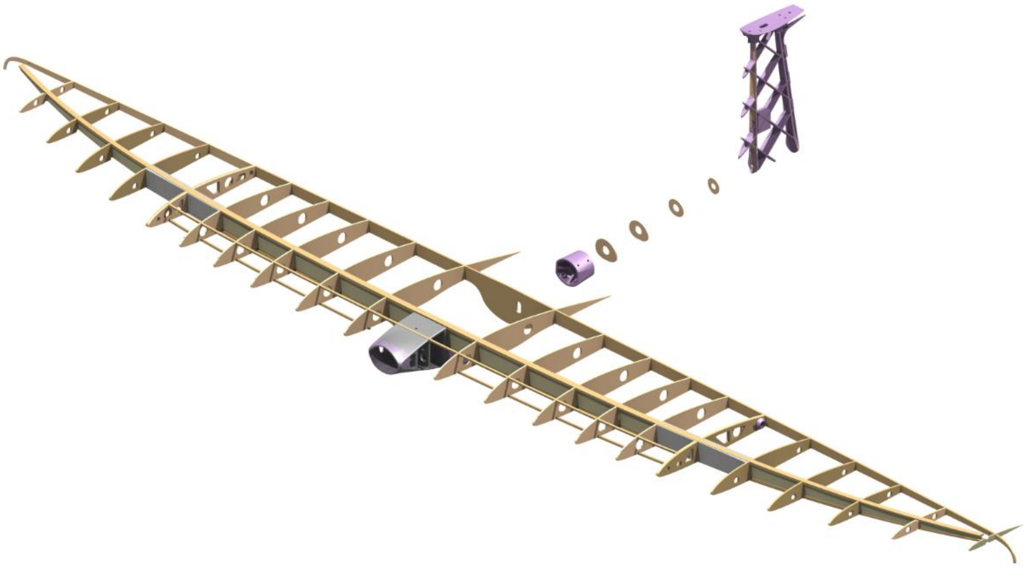

Figure 7: Structural design

3.2.1 Concept

We designed our aircraft using composites. We chose a stressedskin construction with a carbon double layered composite skin and a wooden frame. We created the internal structure from balsa, spruce and plywood parts. In some places, we also used 3D printing, especially on the fuselage and wing joints.

3.2.2 Wing

The wing was designed with CFRP skin and wooden supporting structure. It consist of three parts, one midwing section and two wingtips. The wingtips are removable so that we meet the size requirements. They are connected to the midwing section by aluminium pipes which are inserted into 3D printed components. The main wing spar caps are made from spruce and the spar web is made out of balsa. The spar web is divided into segments between the ribs. The spar caps consist out of a single piece. All ribs are made out of balsa, with the exeption of the two outermost midwing ribs which are made out of plywood. The top skin of the wing also features lockable doors to load and unload cargo

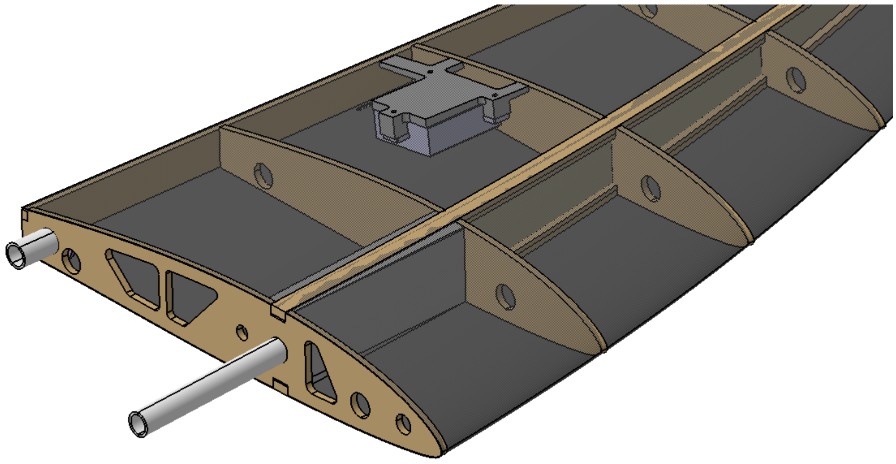

Figure 8: Wingtip structure

3.2.3 Fuselage

The fuselage is of relatively simple design. It consists of a carbon skin, which structuraly handles most of the stress. On certain areas it is also reinforced with balsa bulkheads, adding extra structural rigidity. It is separated into two separate parts, one in front of the wing, one behind it. They are both connected to the centerplane via 3D printed interlocking rings and secured in place with bolts.

3.2.4 Tail

The T-shaped tail also features a stressed skin, internally reinforced with a 3D printed grid-like frame. It also houses the rudder servo. The rudder skin is made of two molded parts. Each part also forms the rear section of the fuselage. The elevator connects on top of the rudder to the previously mentioned frame.

3.2.5 Landing gear

The main landing gear connects to the wing directly in between the ribs. The nose gear is connected to the front of the centerplane. It is inserted to a 3D printed housing, which also doubles as the mounting ring for the front section of the fuselage.

3.3 Propulsion system

We tested the propulsion system configuration as you can see in the graph in section 8.1.

The receiver is to be powered by the main battery, via the use of a voltage converter.

Components	Type
Battery	3s Gens-Ace
Propeller	APC 10x6
Motor	Servo motors AXI 2826/10 GOLD LINE V2
Regulator	Flycolor 40A ESC BEC 5V/3A

Table 6: Propulsion system

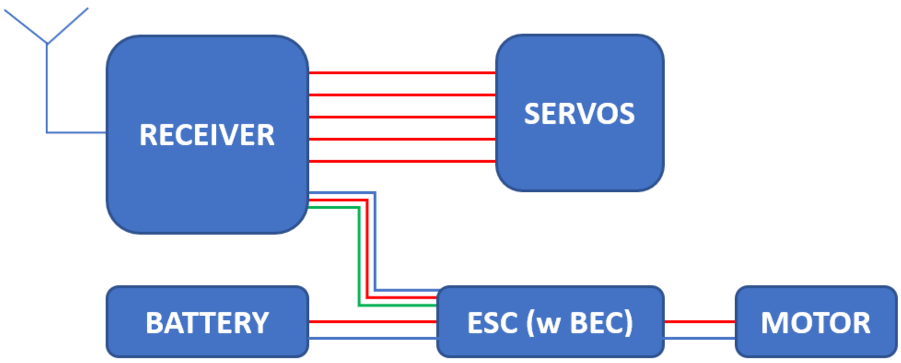

Figure 9: Propulsion electrical circuit scheme

4. Loads and environment assumptions

To perform the analysis, it is necessary to determine assumptions, which can be deduced from geographical location and season, also from the weight of the airplane etc.

During the design process of our aircraft, we considered various natural conditions the aircraft will face. The table below shows the range of different conditions and the usual values. (sources: windfinder.com, climatestotravel.com)

	Temperature	Rainfall	Wind	Atm. Pressure
Range	18 ÷ 24 °C	0-15 mm (40%)	4-6 m/s	1014 ÷ 1018 hPa
Estimated value	21 °C	0 mm	5 m/s	1016 hPa

Table 7: Environment assumptions

Landing shock: It is imperative to dimension the landing gear and the landing gear mounting to withstand the landing shock. An important input of the LG dimensioning is the quality of runway surface. From pictures provided in Participant Handbook [5] we perceived that runway conditions are relatively harsh (grass surface). Considering this we increased size of landing gear wheels and adapted the suspension (more in section 3.1.5).

Inertial forces: This parameter affects the forces that will act on the aircraft. The strongest inertial forces are created by gusts of wind. Therefore they were considered in the flight envelope (section 9.1.1).

5. Aerodynamic design

5.1 Wing Airfoil selection

We performed an analysis of approx 130 low velocity (Re) airfoils in XFLR for Reynolds number values between $2 \cdot 10^5$ and $1 \cdot 10^6$. The parameters of the analysed airfoils were limited by following constraints which we came up with to filter out unsuitable candidates:

- $C_{L\,max}$ in stall speed (Re = 200 000)
- C_D in cruise mode (C_L=0,4; Re = 400 000)
- $(C_L/C_D)_{max}$ (Re = approx 300 000)
- Thickness 8 – 12 %
- max Camber 2,5 – 4,5 %

	A	B	C	D	E	F	G	H	I	J	K	L	M	N	O
1															
2		AIRFOIL	Re/10^6	Alpha ClMa	Cl ma	Alpha Cl/CD ma	Cl/CD ma	Alpha Cl0	Cl04	CD (Cl=0,4	Alpha Cl=	Thickness	at	Camber	at
3		E392 (10.15%)	0.20	9.1380	1.80	3.6880	62.8547	-7.4880	0.4000	0.0824	12.5200	12.52	35.44	2.25	42.25
7		FX 63-137 13.7% smoothed	0.20	6.2520	1.80	3.9420	72.6612	-5.6960	0.4000	0.0744	11.9360	13.08	27.13	9.72	41.64
18		S1210 12%	0.20	7.1880	1.80	6.5050	85.4617	-3.3530	0.5600	0.0158	-5.5930	12.00	34.13	5.02	34.23
19		S1223	0.20	5.5780	1.80	3.1590	71.6253	-3.2260	0.4000	0.0569	-6.9220	12.14	30.86	3.74	40.07
22		S1223 RTL	0.20	6.5020	1.80	3.5900	58.1040	-2.3920	0.7000	0.0241	-7.9940	13.51	19.82	8.46	52.85
26		HT22	0.20	8.6090	1.78	4.4240	58.3776	-4.4100	0.4800	0.0641	15.9120	12.84	27.13	0.21	1.40
32		FX60-100 10.0% smoothed	0.20	6.5480	1.74	1.8920	50.5201	-6.0000	0.4000	0.0758	14.2440	14.05	28.15	2.79	42.06
34		FX 60-100 AIRFOIL	0.20	16.4180	1.72	5.9970	90.2439	-3.8030	0.4000	0.0158	-6.7360	13.67	27.96	2.55	41.87
49		USNPS4 (smoothed)	0.20	13.6340	1.64	2.7060	74.3187	-1.1090	0.4200	0.0177	-3.7270	11.94	29.33	2.65	39.04
54		WORTMANN FX 63-137 AIRFOIL	0.20	11.7990	1.62	5.2760	89.0282	-3.9700	0.4000	0.0160	-6.7820	7.27	32.23	3.84	47.05
61		DAE-21 AIRFOIL	0.20	12.5860	1.58	6.6710	90.3226	-1.4690	0.5000	0.0264	10.8860	11.06	27.13	0.13	0.00

Table 8: Sample result of airfoil analysis

According to these criteria 9 airfoils were chosen for later shape optimization.

Airfoil	K3311	MH32	S3002	S7055	SA7035	SD6060	WASP	S8000	SD7000
thickness [%]	11	8,7	9,9	10,5	9,2	10,4	9,35	8,5	8,5
Camber [%]	3,2	2,4	2,3	3,55	2,55	1,85	2,98	2,1	1,46

Table 9: List of chosen airfoils

5.2 Airplane balanced lift line

Determination of balanced lift line was performed according to (ROSKAM, 2000). There were also included flaps and ground effect for take-off flight modes.

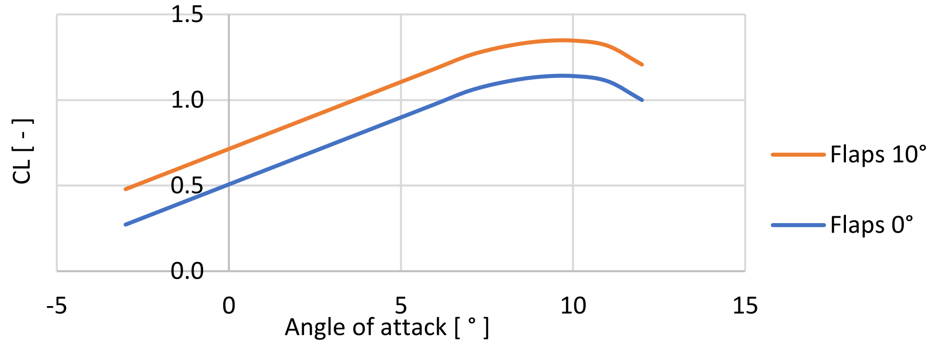

Figure 10: Airplane balanced lift line - middle CG

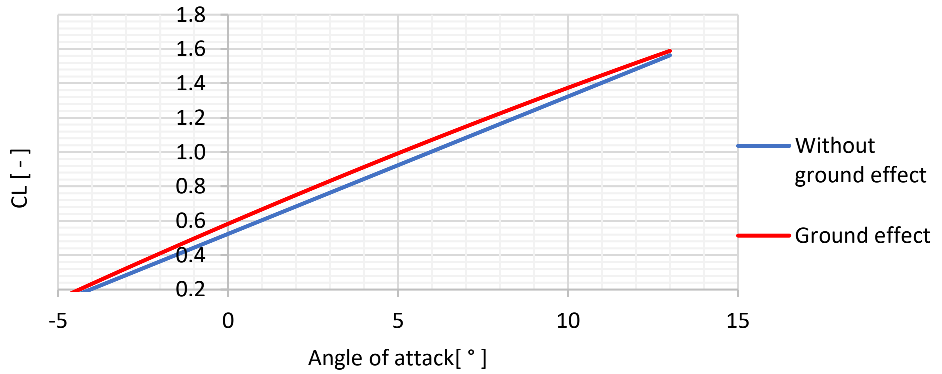

Figure 11: Balanced lift line - middle CG, Flaps 25°

5.3 Airplane drag polar

Airplane drag polar was determined according to (ROSKAM, 2000). There were also included flaps and ground effect for take-off and landing flight modes.

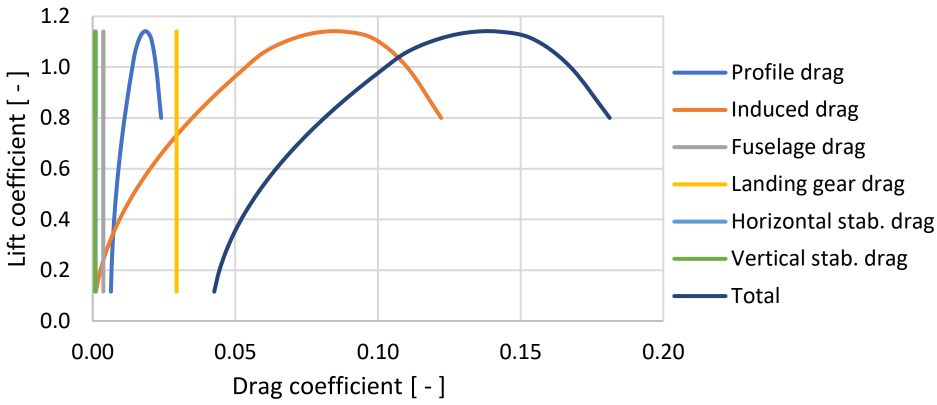

Figure 12: Airplane drag polar - drags

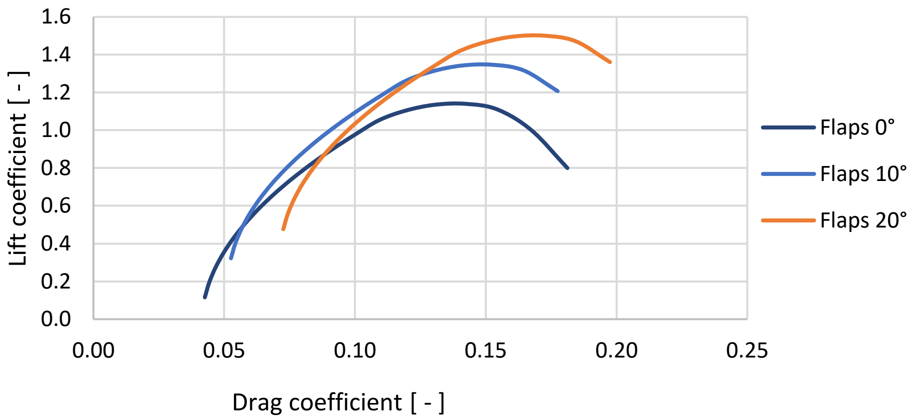

Figure 13: Airplane drag polar - flaps

5.4 Wing lift distribution

Lift distribution was performed using GLAUERT.tcl program. The outcome of the analysis was the position of airstream separation on the wing to avoid unpredictable stall properties. Another outcome was the lift distribution. The results are plotted in the Figure 14: Lift distribution.

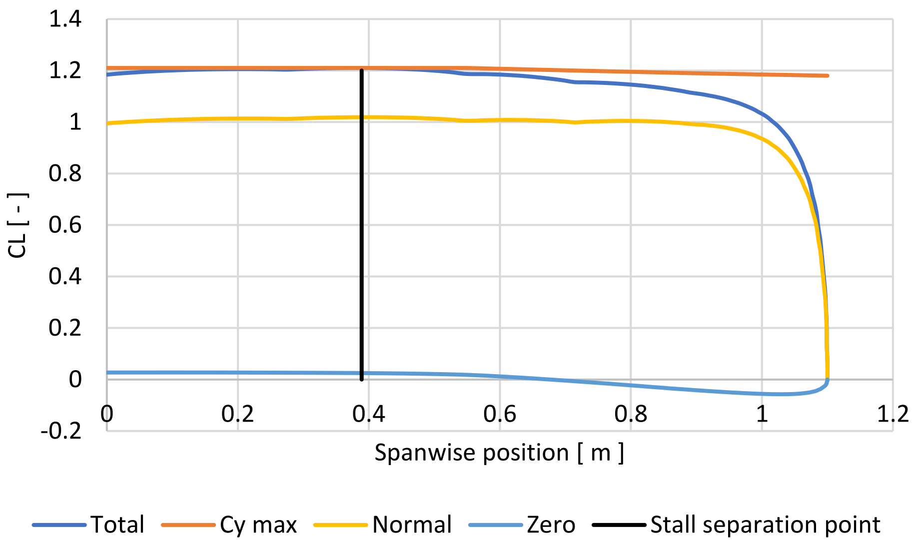

Figure 14: Lift distribution

5.5 Stability and control

5.5.1 Static longitudinal stability

Position of the airplane neutral point was determined according to (TORENBEEK, 1976) Centre of gravity margin was chosen based on experience.

- Neutral point position: 47,8 % $_{MAC}$ (178 mm from leading edge)
- Front CG position static margin: 12 % $_{MAC}$ (140 mm from leading edge)
- Rear CG position static margin: 5 % $_{MAC}$ (164 mm from leading edge)

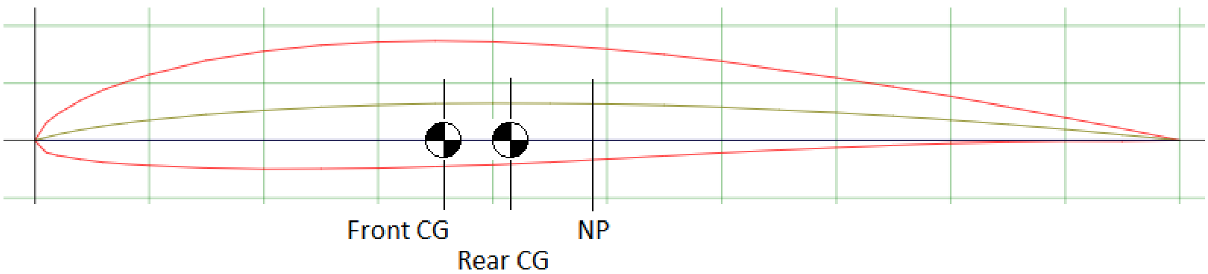

Figure 15: Wing mean aero chord

6. Servo sizing

Servo motors were dimensioned to provide enough hinge-moment to actuate the lift mechanisms. The design conditions for computation are displayed in the table below. Hinge-moments were calculated according to (ROSKAM, 1987).

Having necessary hinge-moments, particular servomotors were chosen. We picked motors with rather high safety factor due to their availability, dimensions and price. Ailerons and flaps are designed to use the same sized servos due to availability and thus we need fewer spare parts on hand and can save some costs, the same applies to the elevator and rudder.

	Depth	Length	Hinge moment	Trans-mission	Servo moment	Type	Servo moment (6 V)	Reserve factor
	(mm)	(mm)	(Nmm)	(-)	(Nmm)	(-)	(Nmm)	(-)
Aileron	77,5	480	330	1,5	220	KST DS135MG	500	2,28
Elevator	69,9	650	300	1,5	200	KST DS135MG	370	2,5
Rudder	77,1	210	106	1,5	71	KST X08H+	370	5,2
Flap	104	441	302	1,5	201	KST DS135MG	500	2,5

Table 10: Servo sizing

7. Flight performance

7.1.1 Take-off performance

Take-off performance was determined as is described in the scheme below. For each configuration the loop of take-off performance is iterated over until all values converge. The result of this step is to prove that the airplane is capable of taking-off from 60 m or 40 m runway.

Distance	Time	Speed	Acceleration	Thrust	Lift	Rolling resistance	AD drag	Sum of forces
x [m]	t (s)	v (m/s)	a (m/s^2)	T(N)	L (N)	RR (N)	D (N)	T (N)
0	0,00	0,00	1,22	13,22	0,00	5,89	0,00	7,33
4	2,56	3,13	1,12	12,59	3,18	5,57	0,32	6,70
8	3,63	4,33	1,07	12,30	6,08	5,28	0,62	6,41
12	4,47	5,22	1,03	12,07	8,86	5,00	0,90	6,17
16	5,19	5,96	0,99	11,87	11,53	4,73	1,17	5,96
20	5,82	6,59	0,96	11,68	14,11	4,47	1,43	5,78
24	6,41	7,15	0,93	11,51	16,61	4,22	1,69	5,60
28	6,95	7,66	0,91	11,36	19,04	3,98	1,93	5,44
[illegible]	[illegible]	[illegible]	[illegible]	[illegible]	[illegible]	[illegible]	[illegible]	[illegible]

Table 11: Result of take-off performance analysis

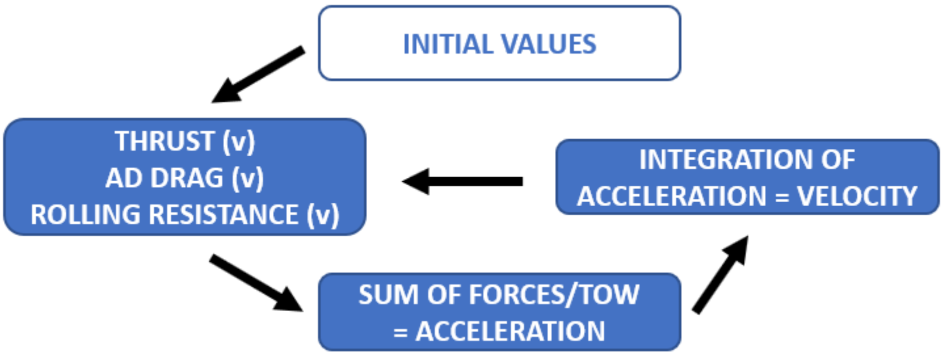

Figure 16: Take-off performance analysis algorithm

7.1.2 Climb rate

Climb rate is an important input for flight score computation and optimization. Calculations for all configurations were performed according to (DANĚK, 2009).

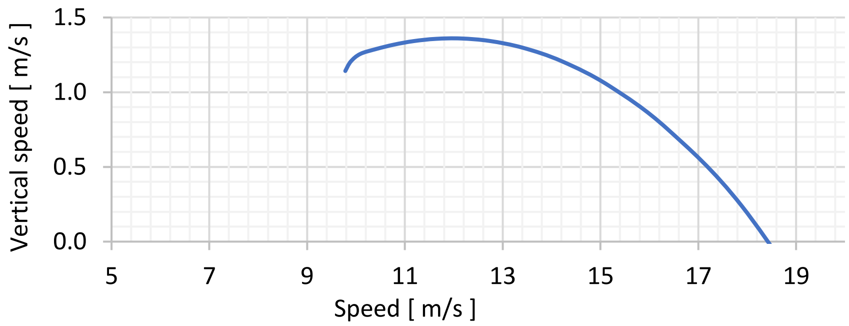

Figure 17: Climb rate

7.1.3 Cruise

Maximum speed of horizontal flight was determined as an intersection of Thrust and Drag curve.

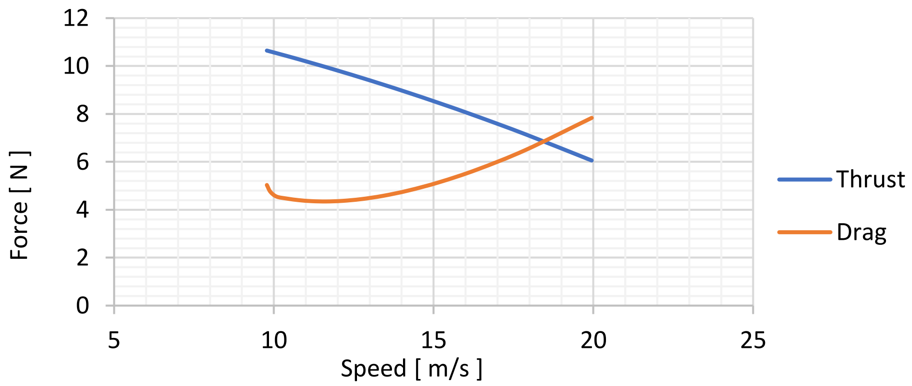

Figure 18: Thrust/drag diagram

8. Scoring optimization

The chart below describes the whole process to obtain optimal aircraft shape.

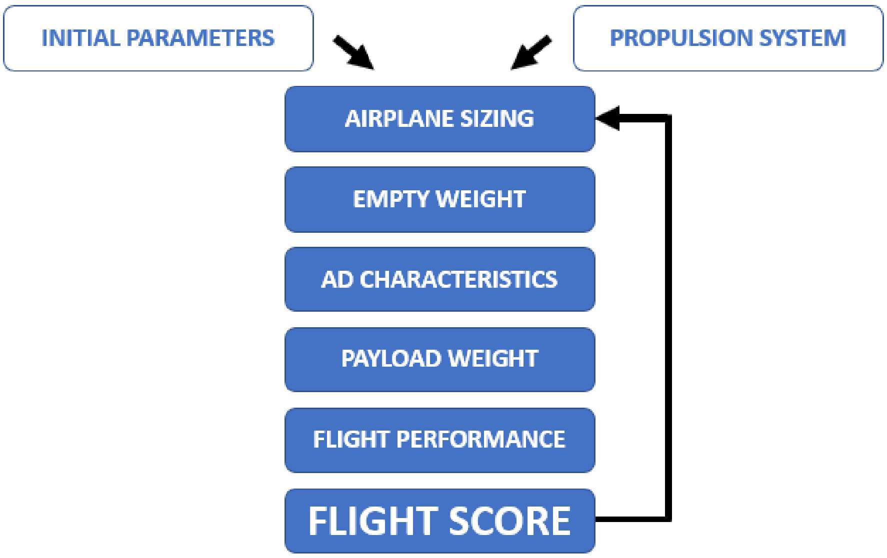

Figure 19: Aircraft shape optimization process

8.1 Propulsion analysis

The dynamic thrust curve of the specified propulsion system (see 3.3 Propulsion system) was measured. Each propeller was measured with fully charged battery 3 times. Results of both propellers were averaged. According to our measurement the APC 10x6 is slightly better in the whole range of speed.

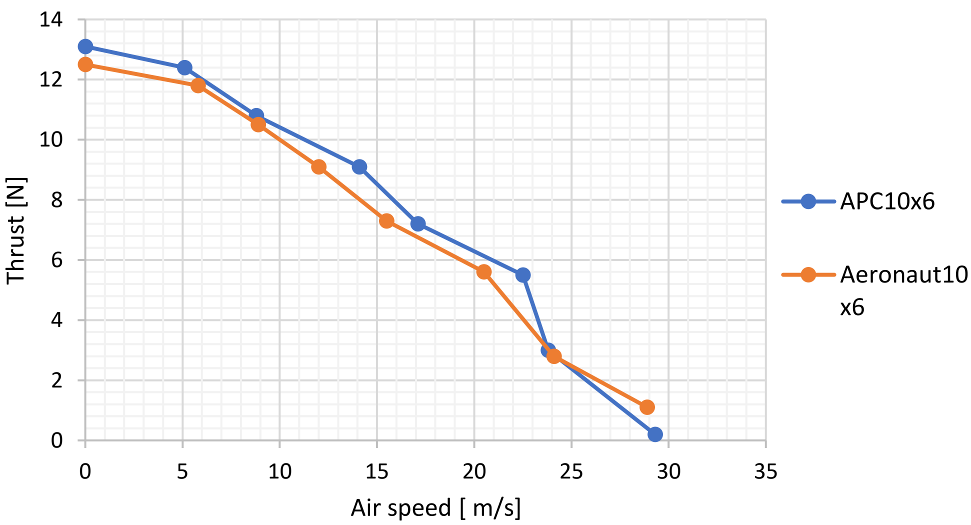

Figure 20: Propeller thrust diagram

8.2 Initial parameters

We initially estimated all parameters for the aircraft shape optimization. Most important parameters as rolling resistance coefficient, flap/aileron relative length/depth or tail volume were estimated based on experience from the past. Minimal wing thickness and depth of middle part of wing was determined to ensure sufficient cargo space. Other limiting factor was a space of rhombus shape box.

8.3 Airplane sizing

There were two independent parameters. Wing area and airfoil shape. We compared 8 airfoil configurations and 3 wingspan configurations to find the optimal aircraft parameters.

The result shows, that the effect of the airfoil upon the flight score is negligible. In general, thinner airfoil allows higher cruise speed, but decreases maximum lift. Nevertheless, the total score is very similar. The impact of configuration choice on the final score less than 1%.

Another requirements within the airfoil selection were relative high thickness and appropriate lift distribution along wingspan to prevent necessity of geometric twisting (may cause manufacturing difficulties).

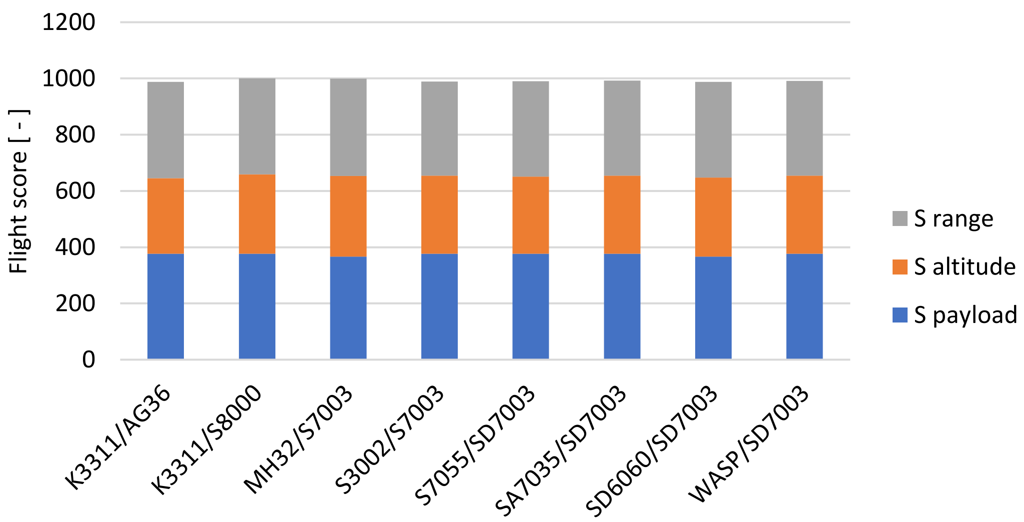

Figure 21: Airfoil influence - 3,5 kg payload, fixed wing

Influence of the wing area describes the chart below. By increasing wing area we can obtain higher flight score, but wing 0,67 m^2 is out of limits of rhombus shape box. So the main goal in this step was to get as much wing area as possible with respecting the rhombus shape box.

There was also included a take-off bonus. It is clear, that in this case it makes sense to reduce some payload and reach a take-off bonus.

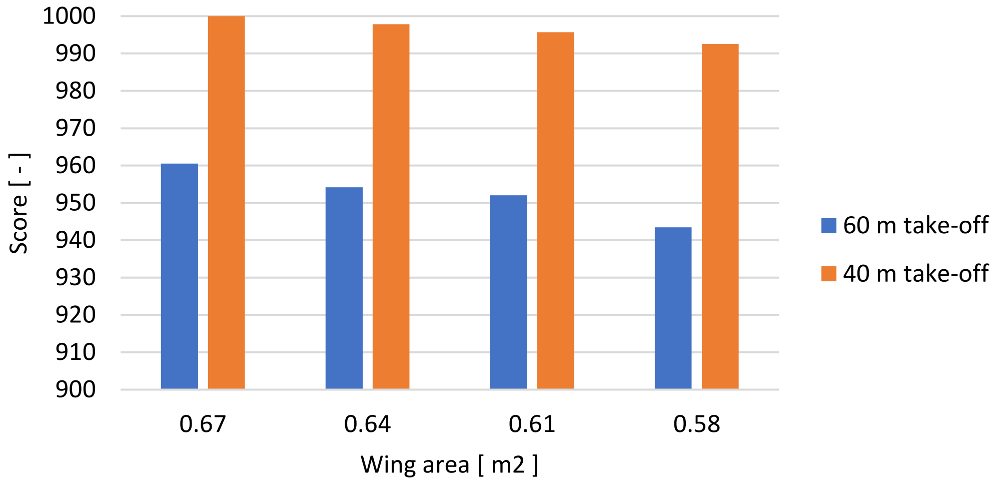

Figure 22: Influence of wing area

8.3.1 Retractable landing gear

The retractable landing gear has been much discussed. A decrease of drag could contribute to better results in climb and cruise flight mode. Of course on the other hand, retractable landing gear would increase empty weight.

Analysis showed, to ensure score advantage, the retractable mechanism would have weight contribution less tdahan 0,35 – 0,45 kg (depends on the payload weight configuration), which is very difficult to achieve even with regard to the reliability of the mechanism on rough runway. This is the main reason why the retractable landing gear was denied

8.4 Empty weight

Based on airplane size and previous experience we estimated the empty weight.

8.5 AD characteristics

Based on speed, wing surface and other important airplane dimensions, the following parameters were determined: drag polar, drag polar including ground effect and flaps, airplane C_L and C_D coeff. during take-off.

8.6 Payload weight

There was a single independent parameter in this step. There were compared 7 payload configurations (from 1 to 3,5 kg).

8.7 Flight performance

Based on previous data, the take-off, climb and cruise performance were determined see ref. Table 10: Servo sizing

Flight performance.

8.8 Score

Based on flight performance and participation handbook [6] the flight score was determined.

We compared: 7 payload weights, 7 airfoils and 3 wing area configurations. Additional parameters were the take-off bonus and fixed/retractable landing gear.

The chart below depicts the result for configuration of 0,64 m^2 wing area, K3311/S8000 airfoil and fixed LG which are the best of all other considered configurations. 3 kg of payload is the limit for successful take-off from 60 m runway and 2,2 kg is limit for 40 m runway to obtain take-off bonus.

The results show, the best configuration is 2,2 kg of payload included take-off bonus.

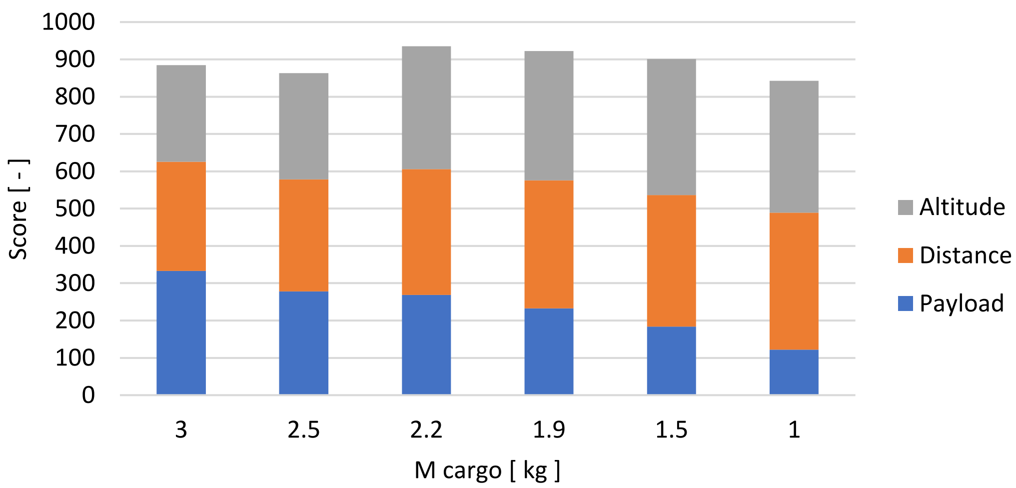

Figure 23: Flight score

9. Structural analysis

9.1.1 Flight envelope

Flight envelope was determined according to modified UL-2 certification specification.

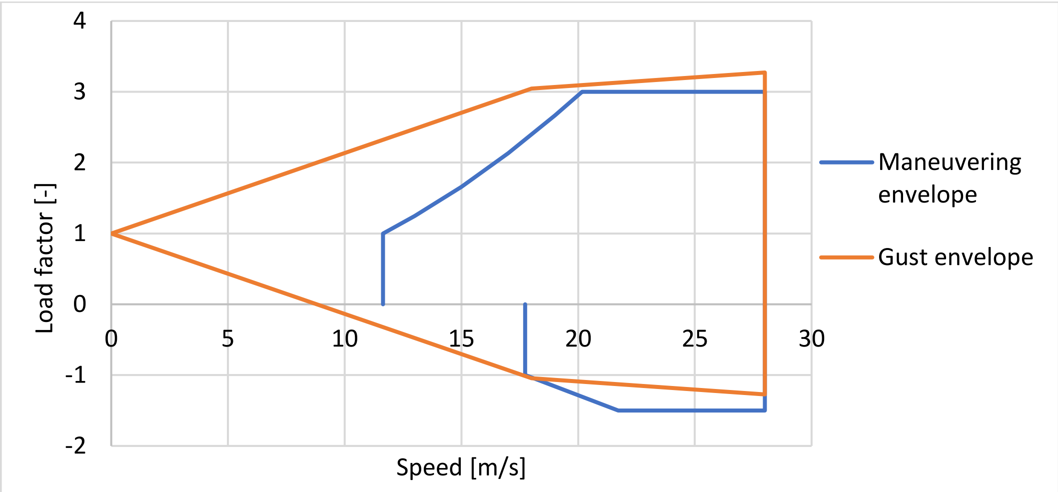

Figure 24: Flight envelope

9.2 Wing load distribution

Wing load distribution was determined as an integration of wing lift distribution including wing weight and payload weigh contribution. In the chart below are shown chosen critical configurations of wing load.

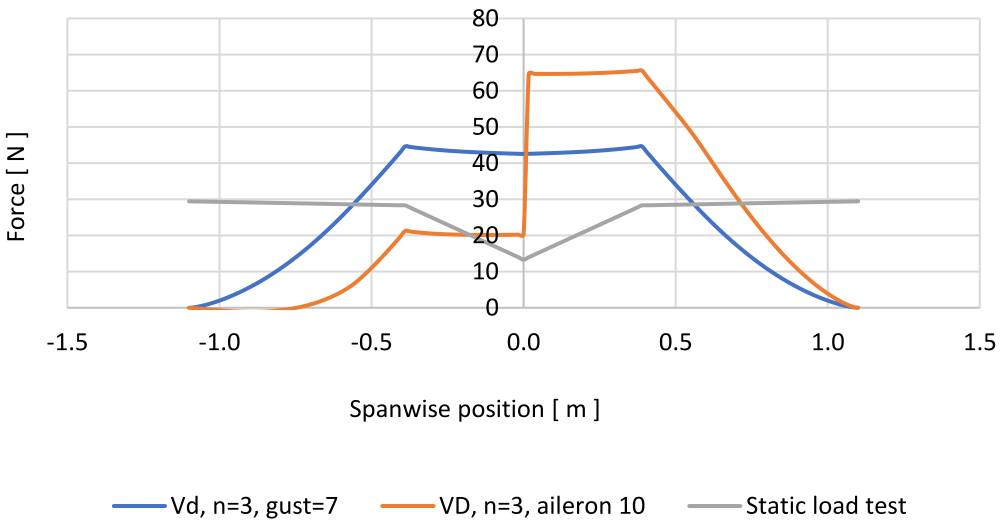

Figure 25: Shear stress distribution

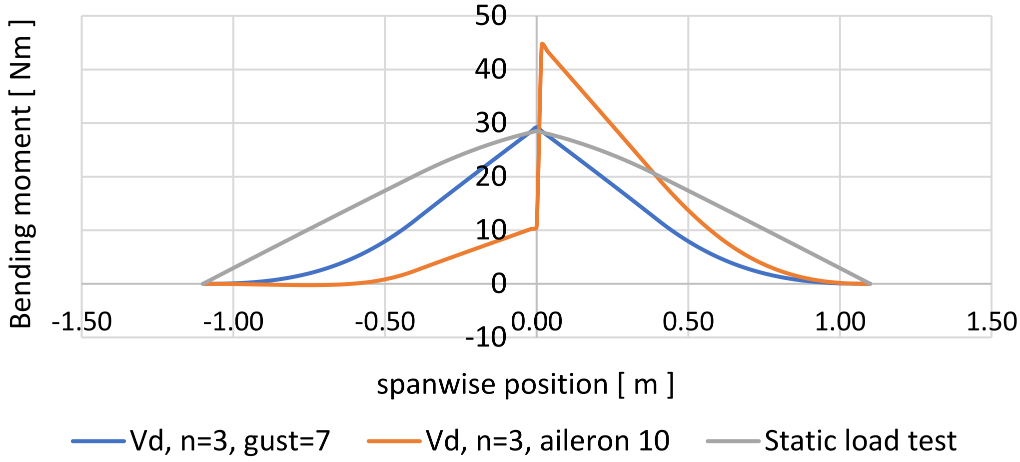

Figure 26: Bending moment distribution

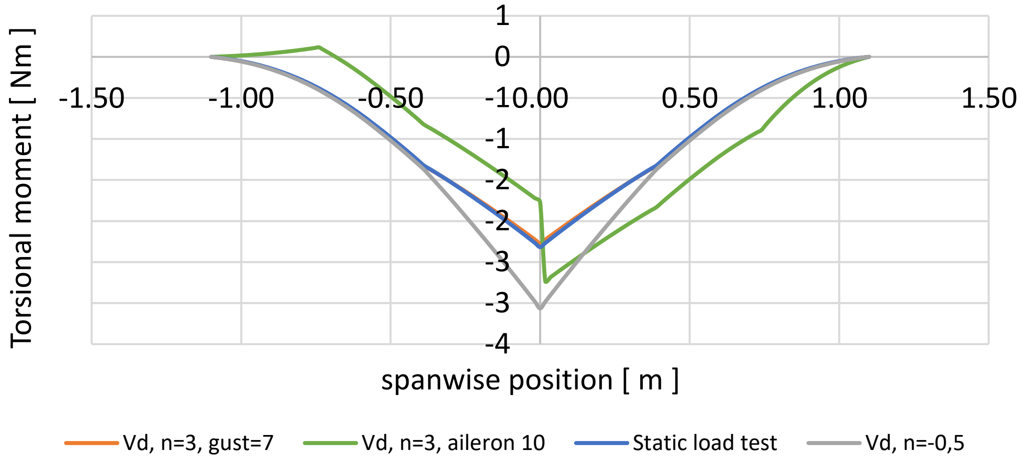

Figure 27: Torsional moment distribution

9.3 Wing main spar stress analysis

There was a performed analysis of wing main spar caps in pull/push stress and analysis of spar web in shear stress. The construction of main spar is described in ref. Structural design

Ultimate compression strength of spruce wood is approx 35 N/mm^2

Ultimate tensile strength of spruce wood is approx 65 N/mm^2

Ultimate shear strength of balsa wood is approx 1,5 N/mm^2

Safety factor of upper spar cap is (1,4 – 2,5)

Safety factor of lower spar cap is (1,85 – 3)

Safety factor of lower spar cap is (1,2 –2,7)

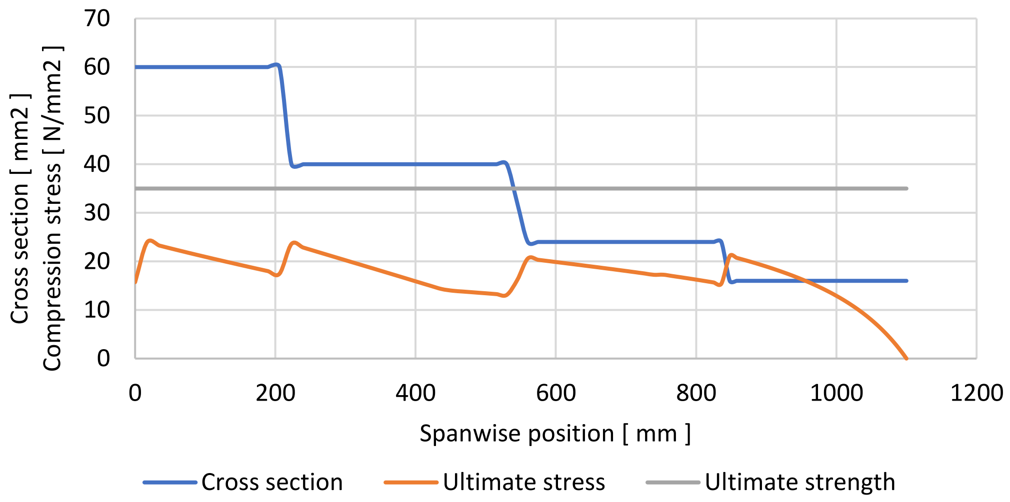

Figure 28: Upper spar cap stress

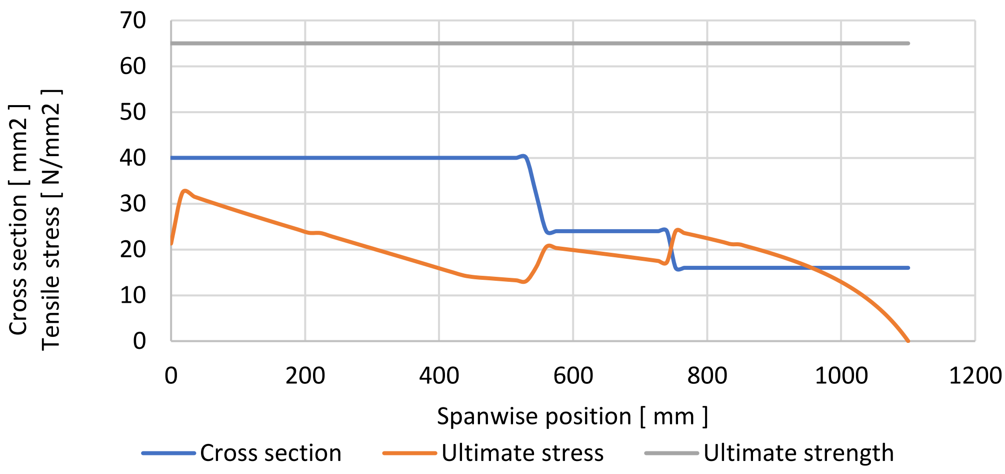

Figure 29: Lower spar cap stress

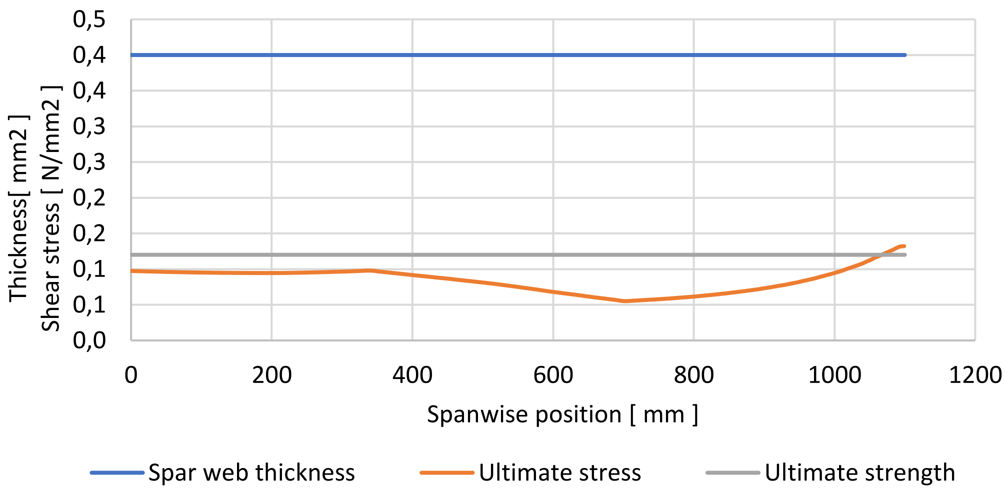

Figure 30: Spar web shear stress

We also performed an analysis of wing bend stiffness. According to results, the maximum deformation during flight (vD, n=3) can occur on the wingtip and it is approx. 60 mm.

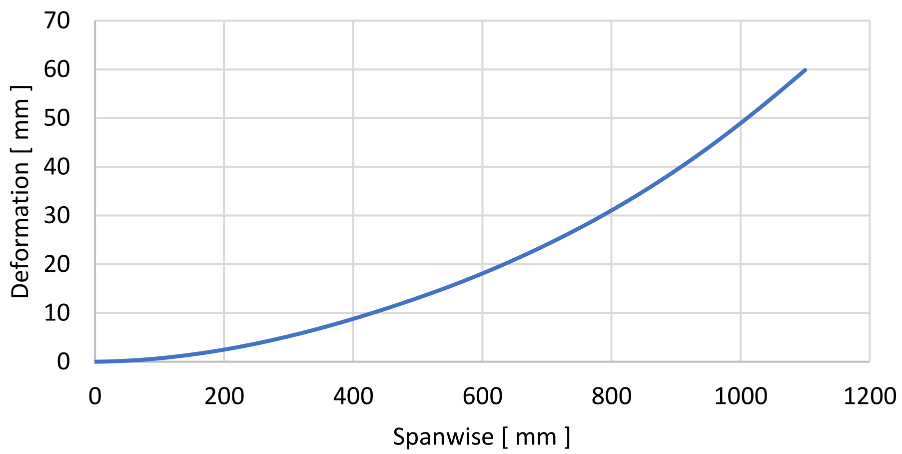

Figure 31: Wing bending deformation

10. Payload prediction

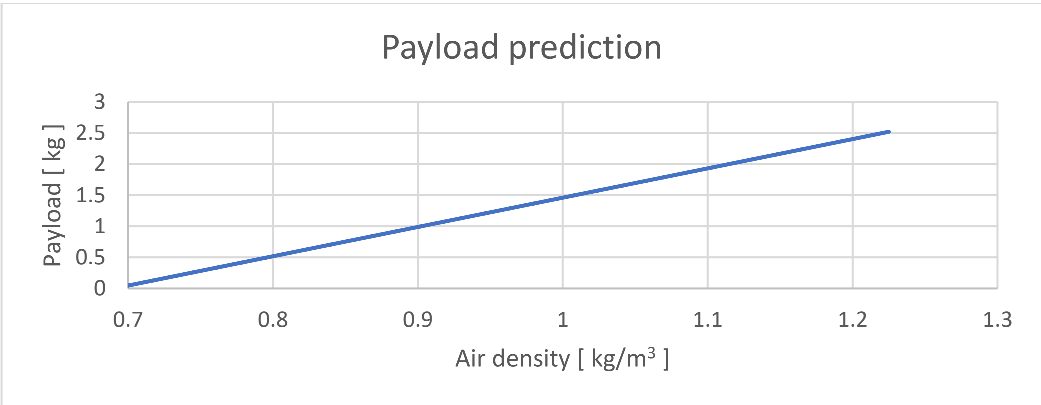

Figure 32: Payload prediction

Payload prediction formula:

$$Y = 4{,}7059x - 3{,}247$$

11. Manufacturing

Main parts of our UAV consist of carbon composite. We are using wet lay-up method which consist of laying cut carbon fibre fabric in mold and then epoxy resin is applied via a brush or a roller after last layer follows epoxy absorbing fabric and the mold is sealed and vacuumed. We are using CNC machined molds made from MDF board and coated with epoxy resin.

Internal structures consist mostly of laser cut balsa wood, plywood or 3D printed structures. For 3d print we use FDM Prusa Mk3s printers on which we mostly print from PLA. We have also access to MJF nylon PA 12 HP printer, which we use for more demanding parts such as connection of the tail to the wing.

12. Outlook

Design process and production of such aircraft is a very complex project which is worth continuity. The aircraft is not only suitable for propagation and marketing purposes but is suitable to be used as a testbed for autonomous flight control systems or as a training aircraft for our team pilots. Moreover, there are plenty of opportunities to further develop production and particular subsystems, e.g. retractable landing gear or various types of empennage.

Structure computations of CFRP parts are very challenging. Next prototypes of our aircraft can be possibly used for mechanical testing.

13. Conclusion

We designed an aircraft that is capable of succeeding in competition of other teams. The main objective was to make the best possible aircraft while keeping the manufacturing process easy. In the designing process, we applied various engineering, designing and manufacturing techniques to ensure the best possible outcome.

Main advantages of our design are the smart storage of cargo in the wing and the right combination of CFRP and ligth wood materials. We also use advanced aditive manufacturing techniques for precise and fast production.

The manufacturing process is being performed under time stress due to fire in our workshop, but we believe that we fulfil our objective and we are ready to challenge our competitors.

14. References

[1] ANDERSON, J. D. (1999). *Aircraft Performance & Design.* University of Minnesota: McGraw-Hill Education.

[2] ROSKAM, D. J. (2000). *Part IV: Layout of Landing Gear and Systems.* Lawrence, Kansas: DARcorporation.

[3] TORENBEEK, E. (1976). *Synthesis of subsonic airplane design.* Delft: Nijgh-Wolters-Noordhof.

[4] ROSKAM, D. J. (1987). *Part VI: Preliminary calculation of aerodynamic, thrust and power characteristics. .* Lawrence, Kansas: DARcorporation.

[5] DANĚK, V (2009). *Mechanika letu I: Letové výkony.* Brno: Akademické nakldatelství CERM.

[6] AkaModell München: *Participation Handbook Version 01.01 07.08.2020*

[7] SLAVÍK, S. (1997). *Stavba letadel. Praha: Vydavatelsví ČVUT.* ISBN 80-01-01671-4.

15. List of tables

16. List of figures

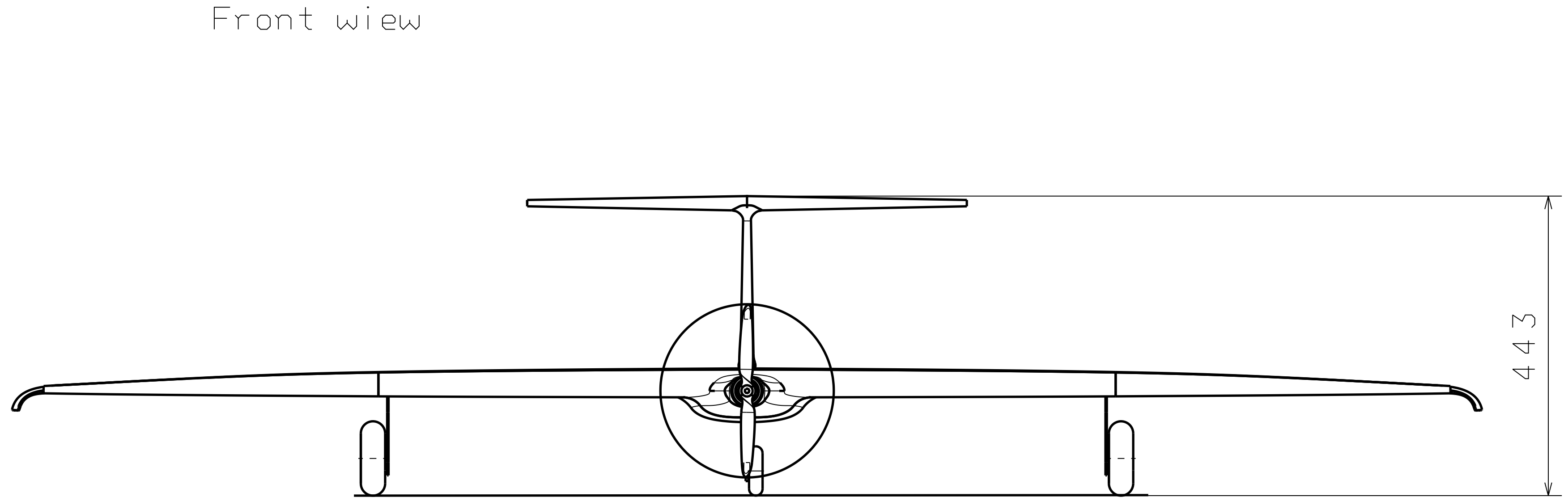

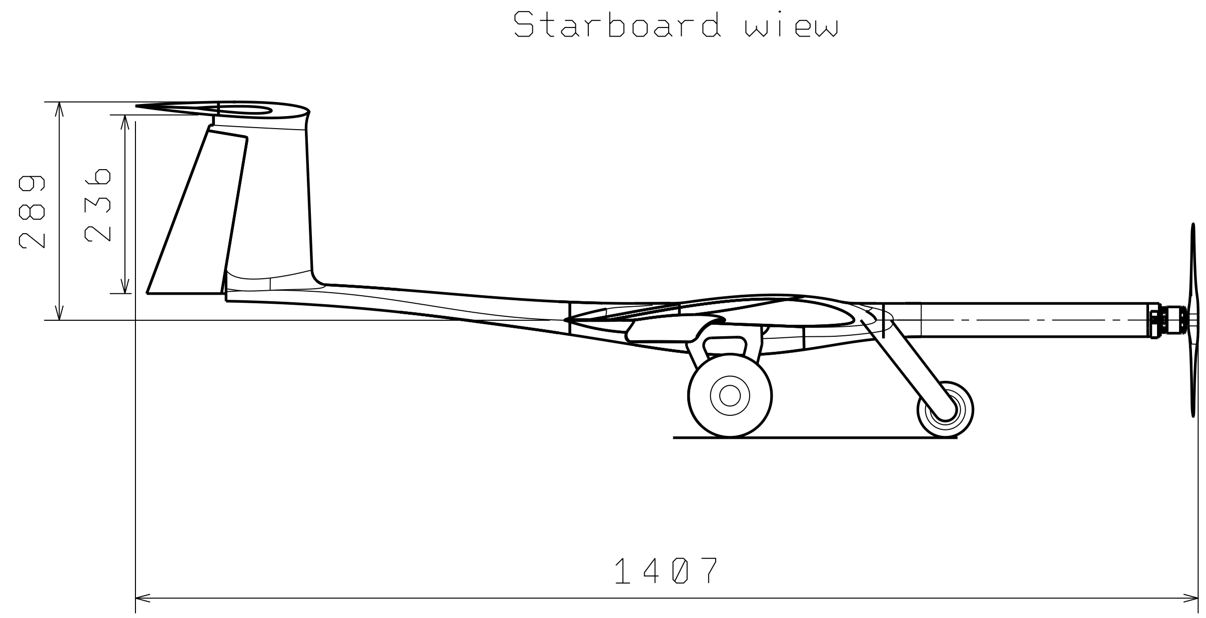

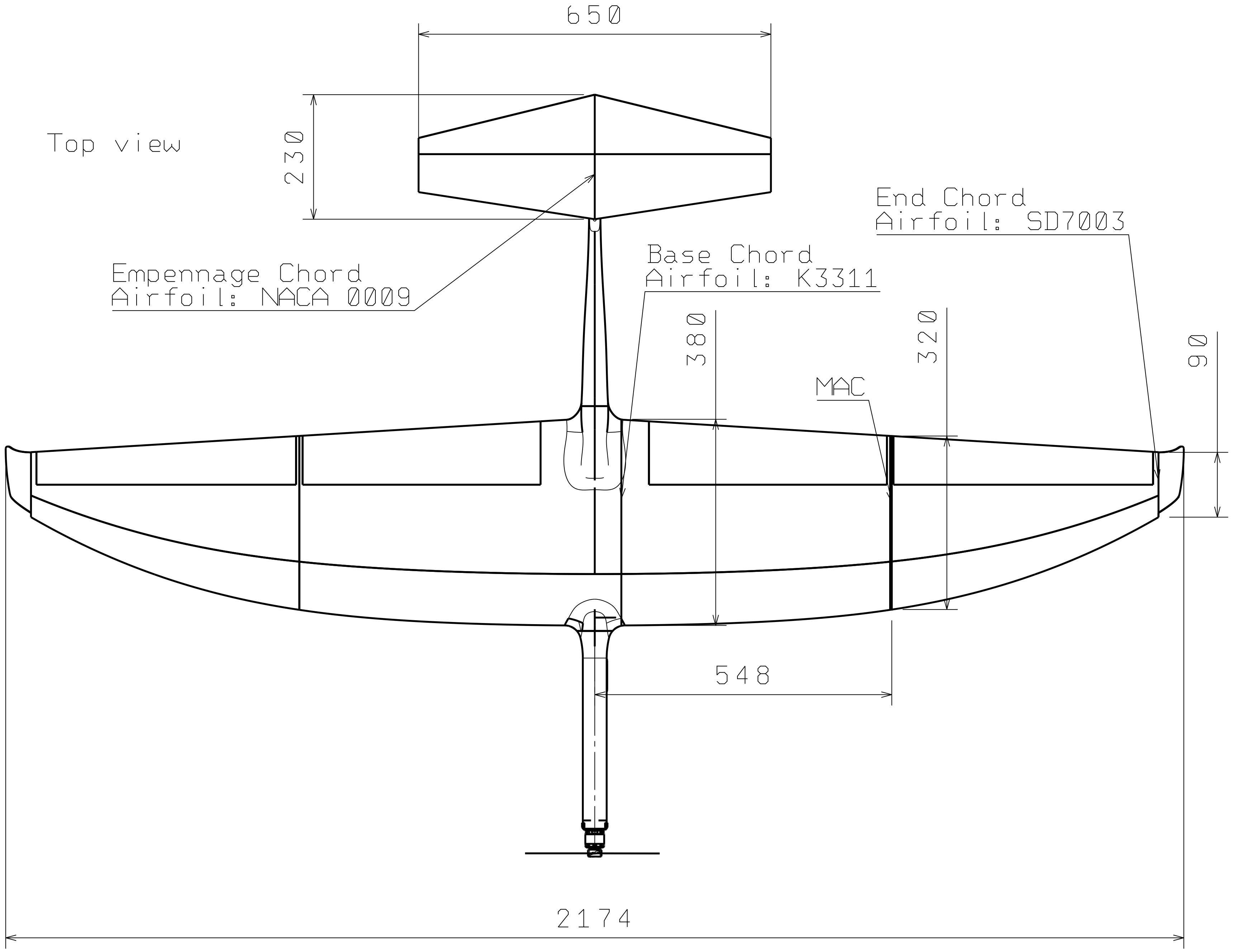

Summary table

Total mass		5,2	[Kg]
Empty mass		3	[Kg]
CG Possstion			
total X pos		138	[mm]
total Y pos		5	[mm]
empty X pos		103	[mm]
empty Y pos		3	[mm]
Used Airfoil	Position	Chord	Airfoil
	0	0,38 m	K3311
	0,55	0,366 m	K3311
	1,05	0,09 m	SD 7003
Empennage airfoil		NACA 0009	
Wing area		0,64	[m^2]
Wingspan		2,12	[m]
Length		1,40	[m]
Horizontal tail volume		650	[mm]
Vertical tail volume		236	[mm]
Elevator lever arm		700	[mm]

Design	Kublak Filip	01-04-22	Scale: 1:10
Drawings	Premysl Cechura	20-04-22	

18 Chicken Wings CTU — A3

Czech Technical Uni. — List: 1/4

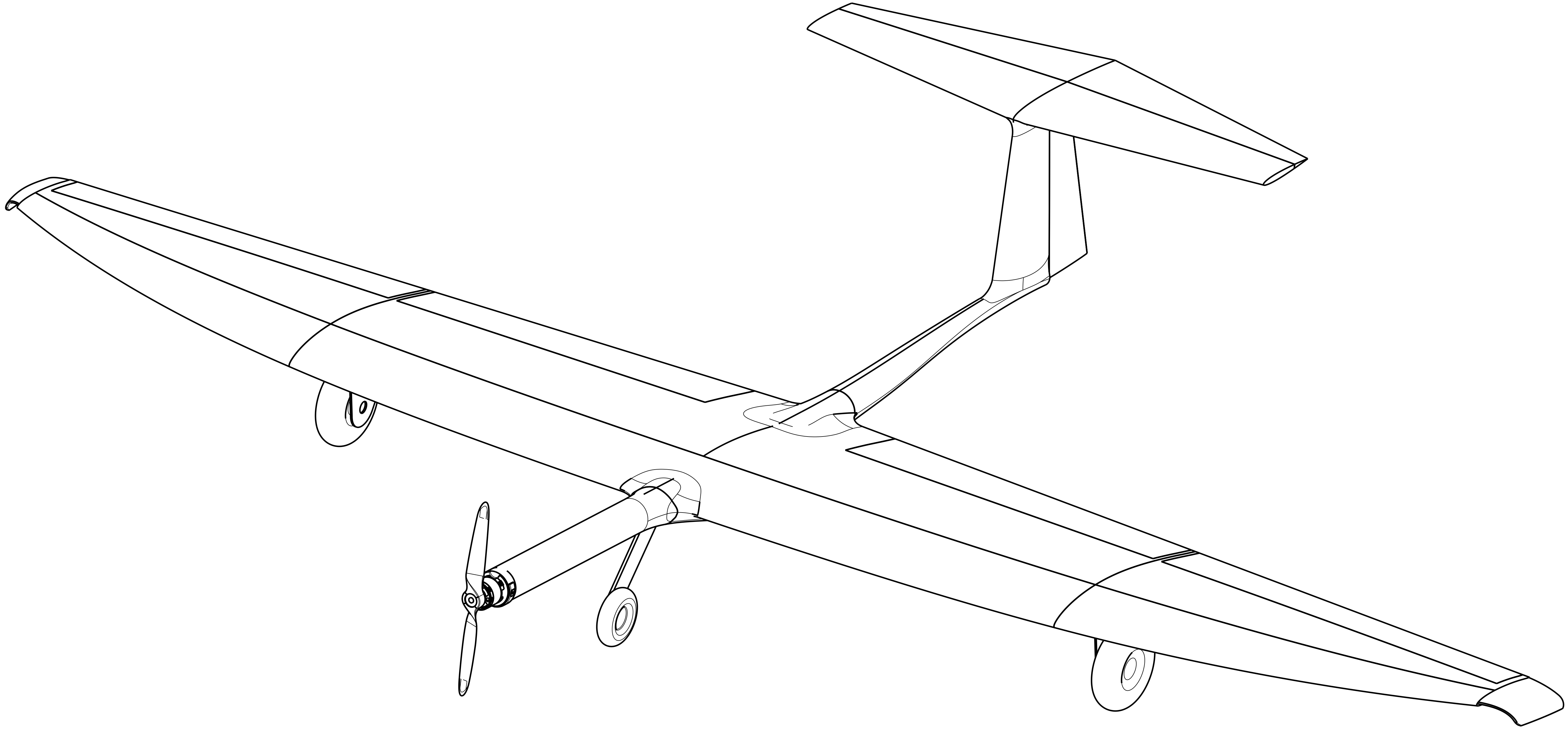

Design	Kublak Filip	01-04-22	Scale: 1:5
Drawings	Premysl Cechura	20-04-22	

18 Chicken Wings CTU	A3
Czech Technical Uni.	List: 2/4

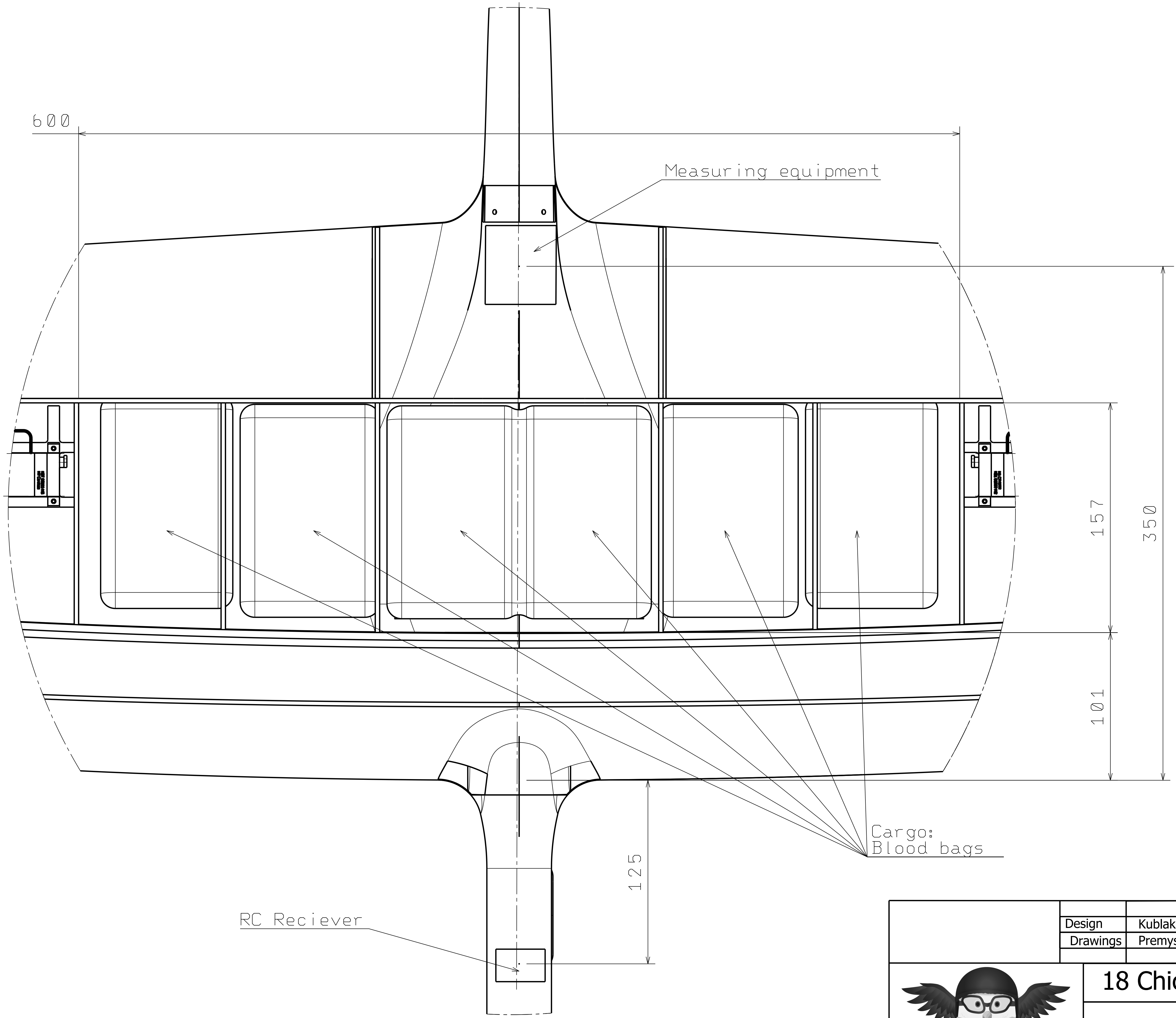

Design	Kublak Filip	01-04-22	Scale:	2:5
Drawings	Premysl Cechura	20-04-22		
18 Chicken Wings CTU			A3	
Czech Technical Uni.			List:	3/4

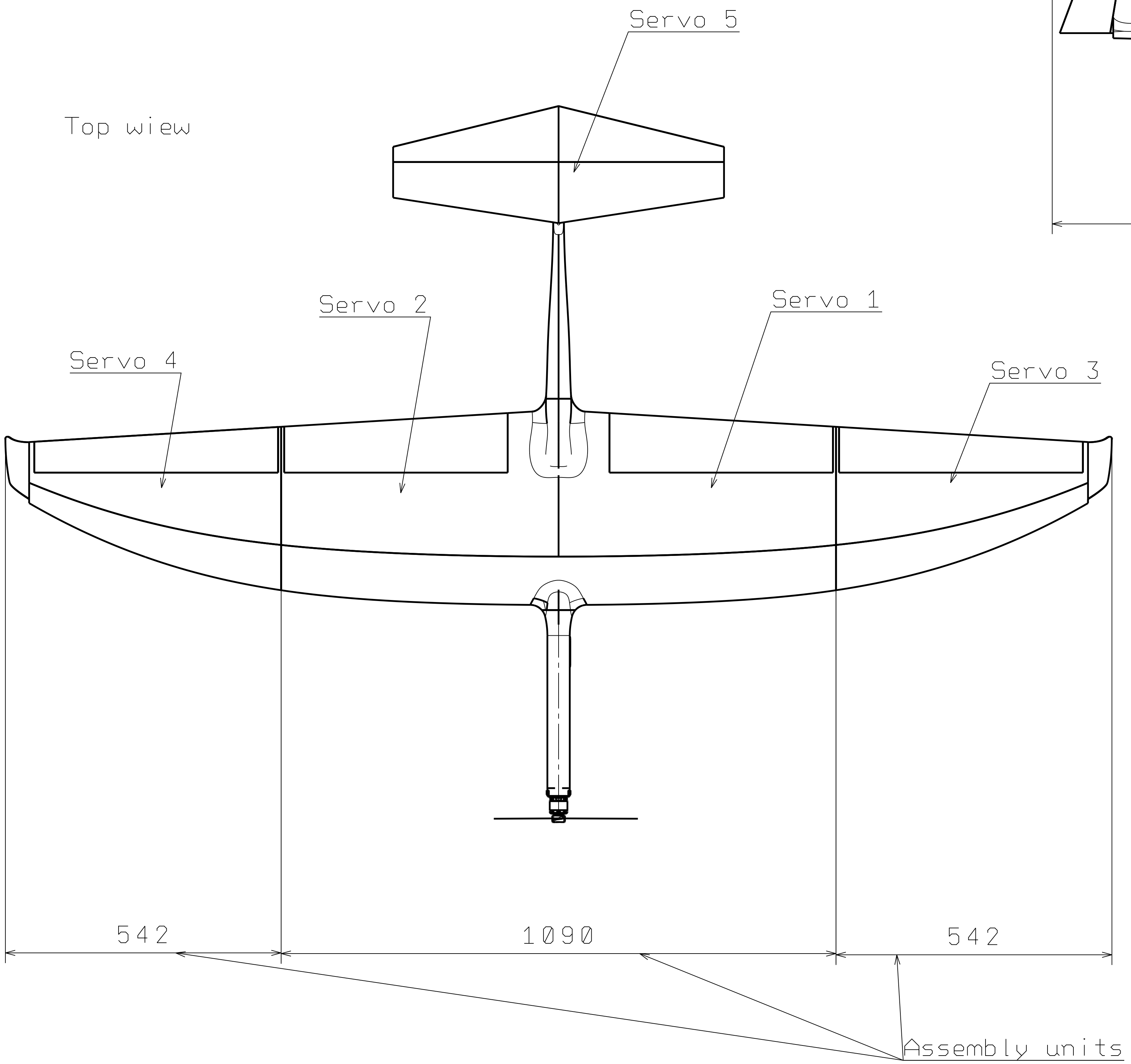

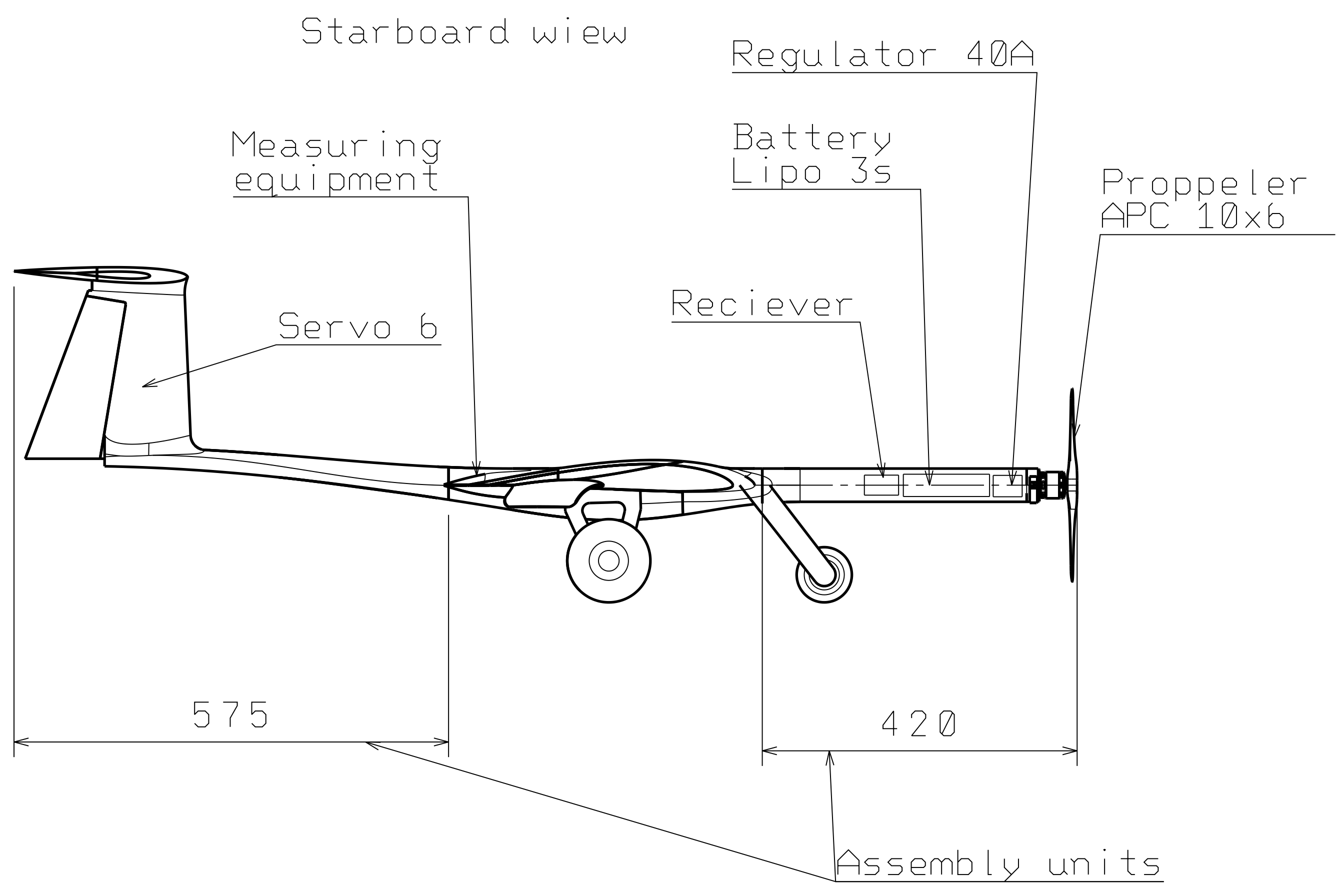

Design	Kublak Filip	01-04-22	Scale: 1:10
Drawings	Premysl Cechura	20-04-22	

18 Chicken Wings CTU | A3

Czech Technical Uni. | List: 4/4